Materials and Design 142 (2018) 203–211

Contents lists available at ScienceDirect

Materials and Design

journal homepage: www.elsevier.com/locate/matdes

Modifying the nanostructure and the mechanical properties of Mo_2BC hard coatings: Influence of substrate temperature during magnetron sputtering

Stephan Gleich [a], Rafael Soler [a], Hanna Fager [a,b], Hamid Bolvardi [b], Jan-Ole Achenbach [b], Marcus Hans [b], Daniel Primetzhofer [c], Jochen M. Schneider [a,b], Gerhard Dehm [a], Christina Scheu [a,d,*]

[a] Max-Planck-Institut für Eisenforschung GmbH, Max-Planck-Straße 1, 40237 Düsseldorf, Germany
[b] Materials Chemistry, RWTH Aachen University, Kopernikusstraße 10, 52074 Aachen, Germany
[c] Department of Physics and Astronomy, Uppsala University, SE-75120 Uppsala, Sweden
[d] Materials Analytics, RWTH Aachen University, Kopernikusstraße 10, 52074 Aachen, Germany

HIGHLIGHTS

- Synthesis of novel Mo_2BC hard coatings by bipolar pulsed direct current magnetron sputtering in an industrial chamber
- Mo_2BC coatings reveal excellent hardness and Young's modulus values
- Mechanical properties depend on on the nanostructure
- Nanostructure evolution from partially short-range ordered to fully crystalline with increasing substrate temperature.

GRAPHICAL ABSTRACT

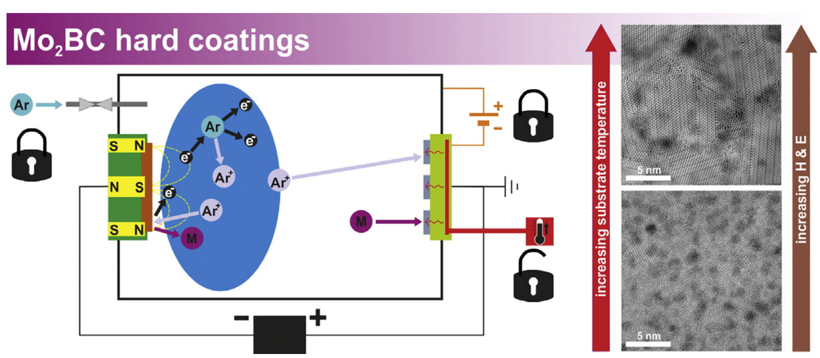

ARTICLE INFO

Article history:
Received 22 September 2017
Received in revised form 12 January 2018
Accepted 16 January 2018
Available online 2 February 2018

Keywords:
Mo_2BC hard coating
Direct current magnetron sputtering
Substrate temperature
Transmission electron microscopy
Nanostructure evolution
Mechanical properties

ABSTRACT

A reduction in synthesis temperature is favorable for hard coatings, which are designed for industrial applications, as manufacturing costs can be saved and technologically relevant substrate materials are often temperature-sensitive. In this study, we analyzed Mo_2BC hard coatings deposited by direct current magnetron sputtering at different substrate temperatures, ranging from 380 °C to 630 °C. Transmission electron microscopy investigations revealed that a dense structure of columnar grains, which formed at a substrate temperature of 630 °C, continuously diminishes with decreasing substrate temperature. It almost vanishes in the coating deposited at 380 °C, which shows nanocrystals of ~1 nm in diameter embedded in an amorphous matrix. Moreover, Argon from the deposition process is incorporated in the film and its amount increases with decreasing substrate temperature. Nanoindentation experiments provided evidence that hardness and Young's modulus are modified by the nanostructure of the analyzed Mo_2BC coatings. A substrate temperature rise from 380 °C to 630 °C resulted in an increase in hardness (21 GPa to 28 GPa) and Young's modulus (259 GPa to 462 GPa). We conclude that the substrate temperature determines the nanostructure and the associated changes in bond strength and stiffness and thus, influences hardness and Young's modulus of the coatings.

* Corresponding author at: Max-Planck-Institut für Eisenforschung GmbH, Max-Planck-Straße 1, 40237 Düsseldorf, Germany.
E-mail address: c.scheu@mpie.de (C. Scheu).

https://doi.org/10.1016/j.matdes.2018.01.029

1. Introduction

Mo_2BC is a wear resistant hard coating material, which can be applied as a protection layer for tool steels. *Ab initio* calculations for Mo_2BC predicted an elastic modulus as high as 470 GPa as well as moderate ductility, which reduces the probability of crack formation and propagation [1]. The excellent theoretically predicted mechanical properties were confirmed by nanoindentation experiments conducted on a Mo_2BC thin film deposited on an Al_2O_3 (0001) substrate at 900 °C using direct current magnetron sputtering (DCMS) [1].

Bolvardi et al. [2] reduced the synthesis temperature of Mo_2BC hard coatings. They achieved deposition onto technologically relevant metallic substrate materials by utilizing high-power pulsed magnetron sputtering (HPPMS) at temperatures ranging from 300 °C to 700 °C. X-ray diffraction (XRD) confirmed that crystalline Mo_2BC was obtained at substrate temperatures higher than 380 °C using HPPMS. This significant reduction in synthesis temperature is facilitated by ion bombardment induced surface diffusion, where film forming ions are utilized in addition to Ar^+ [2].

Buršík et al. [3], Zábranský et al. [4], and Buršíková et al. [5] analyzed the influence of the target material as well as different deposition parameters such as bias voltage, deposition time and substrate temperature on the mechanical properties of Mo-B-C hard coatings. An increase in Young's modulus, from 272 GPa [4] to 462 GPa [5], and in hardness from, 19 GPa [4] to 32 GPa [5], is reported for deposition temperatures ranging from room temperature to 500 °C, respectively. The highest Young's modulus of 500 GPa was reported by Zábranský et al. [6] for a Mo-B-C coating, which was initially grown without applying temperature to the substrate, followed by annealing at 1000 °C.

Thus, much effort has been expended until now to analyze the mechanical properties of Mo_2BC with respect to the deposition technique utilized. However, detailed and atomically resolved analyses of the nanostructure of hard coatings in general, and of Mo_2BC hard coatings in particular, by transmission electron microscopy (TEM) have been rare. In the case of Mo_2BC, first approaches have been pursued by Buršík et al. [3] and Zábranský et al. [4] who characterized Mo-B-C coatings using TEM along with nanoindentation and XRD. Depending on the synthesis condition used, the microstructure of the films showed either fully amorphous character or nanosized columnar grains embedded in an amorphous matrix. In a previous work [7], we analyzed a Mo_2BC coating deposited by bipolar pulsed direct current magnetron sputtering (DCMS) on Si (100) substrates at 630 °C. The coating consisted of densely arranged, textured, columnar grains with a grain diameter of around 10 nm. The grains were ordered in bundles sharing the same crystallographic orientation in the growth direction. Moreover, lattice defects were detected, for example stacking faults and Ar-rich Mo-B-C clusters, which modify the atomic structure [7].

In this study, we address the nanostructure evolution of Mo_2BC coatings as a function of the substrate temperature T_s, ranging from 380 °C to 630 °C. The observed nanostructure is correlated with the mechanical properties.

2. Experimental methods

Deposition of Mo_2BC coatings was performed by bipolar pulsed DCMS in an industrial CemeCon 800/9 deposition chamber. 2 in. Si (100) wafers used as substrates were cleaned and degreased with methanol in an ultrasonic bath for 5 min followed by drying with Argon gas. Afterwards, they were mounted onto the stationary anode. A rectangular $88 \times 500\ mm^2$ Mo_2BC compound target from Plansee Composite Materials GmbH was used, facing the substrates at a distance of 100 mm. Samples were deposited at four different substrate temperatures, namely 380 °C, 480 °C, 580 °C, and 630 °C. For comparison with previous studies [2], the lowest substrate temperature of 380 °C was chosen and increased in 100 °C steps up to 580 °C. The final temperature increment was 50 °C, as the maximum substrate temperature possible with the deposition chamber used is 630 °C. Further deposition parameters are listed in Table 1. After deposition, cooling of the samples was controlled by argon flow and circulation in the chamber with a cooling rate of approximately 2.5 °C/min. The thickness of the samples is between 3.6 and 3.9 μm as determined by cross-sectional scanning electron microscopy. In the following sections, the four different coatings are referred to, according to the applied substrate temperature, as Coating_380, Coating_480, Coating_580 and Coating_630 (all values in °C).

Phase analysis was performed by XRD in Bragg–Brentano geometry on a Seifert Type ID3003 diffractometer. The device was equipped with a Huber 2 circle goniometer and operated with Co K_α radiation. θ–2θ scans were acquired over a 2θ range from 20° to 130°. The measurements were performed with a θ offset of 3° to obtain diffraction information from the coating and exclude contributions from the substrate.

Nanoindentation experiments were performed using an Agilent G200 device with a Berkovich tip to understand the mechanical properties of the Mo_2BC coatings, including Young's modulus and hardness. For each sample, 20 quasi-static indentations were carried out with a maximum indentation depth of 300 nm, corresponding to a film thickness of approximately 8%, and at a strain rate of 0.05 1/s. Young's modulus and hardness were calculated following the Oliver and Pharr method [8]. The influence of the substrate on the Young's modulus was taken into account by applying the method established by Hay and Crawford [9], resulting in a Young's modulus exclusively of the coatings. Poisson's ratios of 0.28 for Si [10] and 0.26 for Mo_2BC [1] were assumed for the calculations. For more information on the input parameters, the reader is referred to our previous work [7].

Several TEM methods, including conventional TEM, scanning TEM (STEM), selected area electron diffraction (SAED) and electron energy loss spectroscopy (EELS) were performed to analyze the nanostructure of the Mo_2BC coatings in detail. STEM and EELS measurements were carried out on a FEI Titan Themis 60–300 operated at 300 kV and equipped with a high-energy resolution Gatan image filter (Quantum ERS). EELS was performed in dual EELS mode [11], simultaneously measuring the low loss spectrum at 0 eV energy shift with an acquisition time of 0.0001 s and the high loss spectrum at 120 eV energy shift and an acquisition time of 0.1 s. A dispersion of 0.25 eV/channel was chosen and 100 frames per measurement were summed up. The convergence semi-angle α was set to 23.8 mrad and the collection semi-angle was set to a value of 35 mrad. All EEL spectra were corrected for dark current and channel-to-channel gain variation [12]. Moreover, the noise level was reduced in the EEL spectra by applying the Savitzky-Golay filter [13]. SAED and conventional TEM analyses were conducted at 200 kV acceleration voltage with a Philips CM 20 TEM and a Jeol JEM-2200FS. Quantitative grain size and Ar-rich Mo-B-C cluster evaluation were performed on the basis of utilizing contrast differences in the acquired STEM and TEM micrographs. An appropriate threshold of intensity was defined which filtered only the region of interest and masked out the background. Plan-view and cross-sectional TEM samples were prepared using mechanical polishing and final Ar^+ ion milling in a Gatan precision ion polishing system (PIPS II, model 695) [14].

Information on the elemental composition of the coatings was obtained free from standards by elastic recoil detection analysis (ERDA)

Table 1
Parameters used for deposition of the coatings.

Deposition parameter	Value
Base pressure	$<10^{-4}$ Pa
Ar (99.999%) pressure	0.35 Pa
Substrate bias potential	−100 V
Power supply: bipolar pulsed DC (ENI RPG-100E, MKS instruments)	
Time-averaged power density	6.1 W/cm^2
Frequency	50 kHz
Positive voltage	+37 V, 2 μs
Negative voltage	−405 V, 18 μs

with a time-of-flight and energy detector (ToF-E-ERDA) at the tandem accelerator laboratory of Uppsala University. A 36 MeV $^{127}I^{8+}$ beam was used, incident at 67.5° relative to the sample surface and the detector telescope was aligned at a 45° detection angle with respect to the incident beam direction. Details on the gas ionization detection system can be found in the literature [15]. Homogeneous depth profiles were obtained and evaluated using the CONTES code [16] resulting in relative concentrations. It is noteworthy that systematic uncertainties in absolute concentrations derived from ToF-ERDA in the absence of standards may occur. They mainly originate from inaccurate knowledge of the specific energy loss of the constituents and the primary ion in the target. Such possible uncertainties, however, have no impact on relative concentrations as presented in the current work, where counting statistics is the dominant contribution to the achievable accuracy. For details, the reader is referred to the supplements of to Baben et al. [17] or Arvizu et al. [18].

3. Results

The elemental compositions of the coatings were obtained by ERDA. In addition to Mo, B and C, Ar was also considered for the quantification. The results are summarized in Table 2.

Considering only Mo, B and C, the coatings have chemical formulae which slightly deviate from the nominal stoichiometry of Mo_2BC (see Table 2). Mo and B are within the measurement errors consistent with the stoichiometric composition while the C concentration is sub-stoichiometric. The concentration of Ar decreases with increasing substrate temperature. Moreover, a constant O content of <2 at.% was detected in all four coatings as impurity.

Diffraction patterns of the as-deposited coatings are displayed in Fig. 1. The diffraction pattern of Coating_630 (black) is consistent with Mo_2BC (JCPDF: 00-018-0250), confirming an orthorhombic crystal structure (space group *Cmcm*) [19]. The peak intensity at $2\theta = 70.9°$ is higher compared to the other peaks in this pattern. Such a difference in intensity is not observed in powder patterns [19] and thus, does not result from a high scattering cross-section. This peak can be indexed to the (200)/(002) plane of Mo_2BC and indicates a textured growth, which is in line with our previous study [7]. Due to the strong textured character of Coating_630, several Mo_2BC diffraction peaks, such as those arising at 2θ values of 91° and between 37° and 45°, show almost no intensity. The patterns of Coating_380 (green), Coating_480 (blue) and Coating_580 (red) differ from the diffraction pattern of Coating_630. Two broad peaks at 2θ values of 42.5° and 91° can be detected. The intensity of these peaks increases with increasing T_s. These broad peaks originate from an overlap of several diffraction peaks, which can be assigned to Mo_2BC. Although this result is a strong indication of the formation of Mo_2BC crystals, the data cannot be used for a quantitative prediction of the grain size. Furthermore, the (110), (200)/(002), (220), (310) and (330) diffraction peaks of Mo_2BC are not detected at lower T_s (green, blue and red patterns).

A detailed analysis of the nanostructure of the coatings was obtained by TEM investigations. In Fig. 2, dark field (DF) micrographs of Coating_630 (see Fig. 2(a)), Coating_580 (see Fig. 2(b)), Coating_480 (see Fig. 2(c)) and Coating_380 (see Fig. 2(d)) in cross-section are shown. The micrographs were taken in the middle of the coatings relative to the substrate, the growth direction in each micrograph is indicated by an arrow. The bright appearing regions in the micrographs fulfill the diffraction condition for a defined diffraction spot in reciprocal space and are therefore an indication for the crystalline character of the coatings. A columnar grain structure can be clearly identified at $T_s = 630$ °C in Fig. 2(a) with grains extending in the growth direction perpendicular to the substrate. The coatings synthesized at lower T_s also show crystalline features, but the columnar grain structure is less distinctive. In Fig. 2(b) the columnar character is still detectable, but it decreases in Fig. 2(c) and for Coating_380 rather spherical-shaped grains are observed (see Fig. 2(d)). Further TEM measurements revealed that the Si substrate exhibits a native oxide layer. Thus, epitaxial growth can be excluded, as the coating growth initiated on amorphous matter.

Fig. 3 shows bright field (BF) TEM micrographs of the coatings in plan-view. A dense array of columnar crystalline grains with an average diameter of 10.3 ± 3.8 nm were detected in Coating_630 (see Fig. 3(a)) in accordance with our previous study [7]. In Fig. 3(b), the average grain diameter is only 1.9 ± 1.1 nm and the array of grains is less dense, which indicates that the grains are embedded in an amorphous or short-range atomic ordered matrix (see also Fig. 4). Similar results are obtained for Coating_480 and Coating_380 in Fig. 3(c) and Fig. 3(d). The grain size decreases further, in Coating_480 an average grain diameter of 1.5 ± 0.6 nm and in Coating_380 of 1.2 ± 0.4 nm can be detected. The insets in Fig. 3(a)-3(d) show SAED patterns of the coatings, which are acquired in plan-view. The diffraction rings of Coating_580, Coating_480 and Coating_380 exhibit a diffuse character. A non-uniform intensity distribution can be detected on two arcs which can be assigned to the (140)/(041) and (200)/(002) planes of Mo_2BC. A more spotty diffraction pattern can be detected in the case of Coating_630. The diffraction spots are located on arcs and can also be assigned to Mo_2BC. Due to the textured character of Coating_630, in which the crystallites grow in a preferred [100] orientation [7], the (200) plane is oriented almost parallel to the electron beam and therefore cannot be detected.

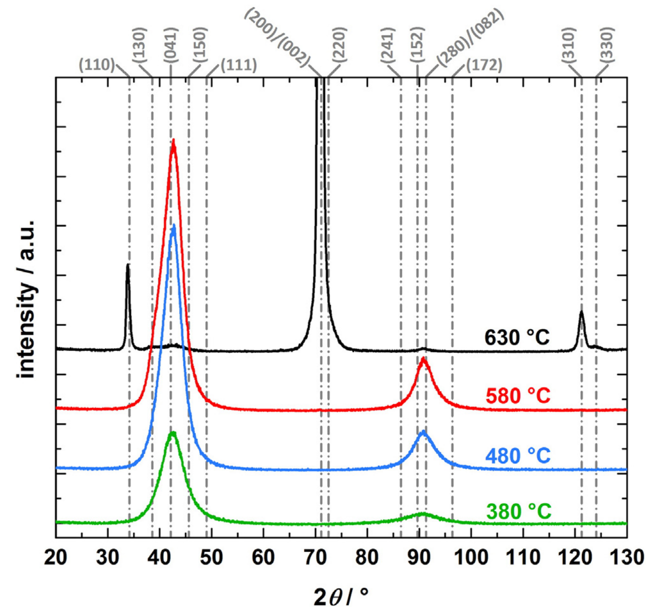

Fig. 1. X-ray diffraction patterns of Mo_2BC coatings deposited on Si (100) substrates at different T_s: 380 °C (green), 480 °C (blue), 580 °C (red), and 630 °C (black).

Table 2
Quantification of elements detected by ERDA. All values are reported in atomic percent (at.%).

Detected element	$T_s = 380$ °C	$T_s = 480$ °C	$T_s = 580$ °C	$T_s = 630$ °C
	Amount in at.%	Amount in at.%	Amount in at.%	Amount in at.%
Mo	50.8 ± 1.4	51.1 ± 1.6	51.5 ± 1.9	49.9 ± 1.8
B	26.5 ± 2.2	24.8 ± 2.2	24.7 ± 2.0	26.0 ± 2.6
C	21.3 ± 1.2	22.6 ± 1.2	22.9 ± 1.3	23.4 ± 1.0
Ar	1.4 ± 0.4	1.5 ± 0.3	0.9 ± 0.3	0.7 ± 0.3
Resulting chemical formulae of the Mo-B-C coatings				
	$Mo_{2.1}B_{1.1}C_{0.9}$	$Mo_{2.1}B_{1.0}C_{0.9}$	$Mo_{2.1}B_{1.0}C_{0.9}$	$Mo_{2.0}B_{1.0}C_{0.9}$

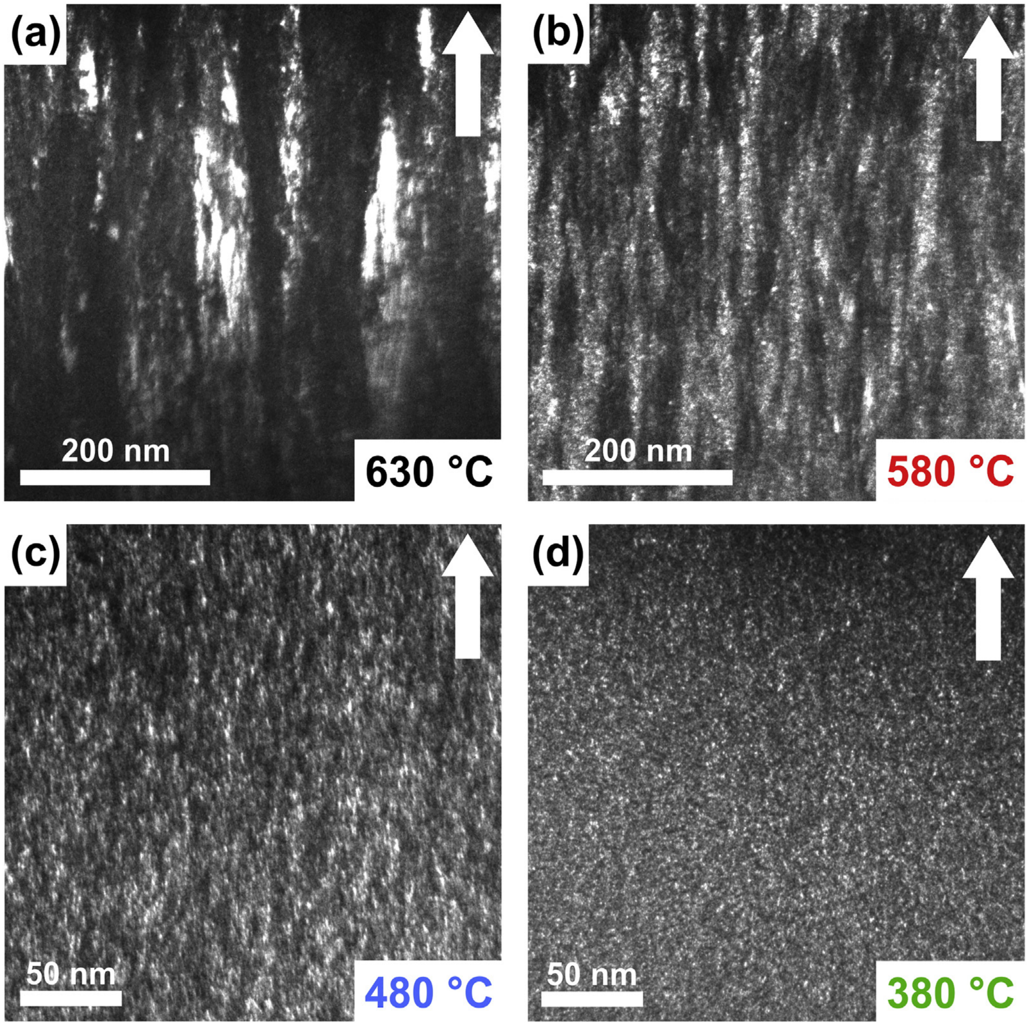

Fig. 2. DF TEM micrographs of Mo_2BC coatings in cross-section deposited at different T_s: (a) 630 °C, (b) 580 °C, (c) 480 °C, and (d) 380 °C. The growth direction is highlighted in each micrograph by a white arrow. Please note the different magnification in (a) and (b) compared to (c) and (d).

Detailed information on the nanostructure of the coatings were obtained by STEM high-angle annular dark field (HAADF) investigations, utilizing the effect of Z contrast, since elements with a higher atomic number Z scatter the incident electrons more strongly. In Fig. 4(a), the atomically resolved nanostructure of Coating_630 is depicted and shows the densely packed grains oriented in [100] viewing direction, which are surrounded by a less ordered grain boundary region. The results are in agreement with our previous studies [7]. By superimposing a simulated structure of Mo_2BC onto the structure of the coating, the bright appearing columns can be assigned to Mo and the dark appearing layers can be assigned to B (see inset in Fig. 4(a)). The B columns are ordered in zig-zag lines in [100] viewing direction and therefore can be detected indirectly, although they appear dark due to the lower atomic number of B. The same applies for C, which is octahedrally surrounded by Mo in the Mo_2BC structure. The intensity of the C column signal is too low to distinguish it from free space between atom columns. Crystalline features can also be detected in Coating_580, Coating_480 and Coating_380 (see Fig. 4(b)-4(d)). The grains for these coatings are smaller in size and do not exhibit a distinct elongation in the growth direction. As a result, several grains overlap in STEM HAADF micrographs, as TEM images are only two-dimensional projections. Furthermore, the degree of crystallinity decreases from Coating_580 to Coating_380. The fraction of short-range atomic ordered matter (amorphous matrix) to nanocrystalline grains increases with decreasing T_s. All four coatings show the existence of dark appearing features, which are homogeneously distributed throughout the analyzed coatings. For each micrograph in Fig. 4, one of these dark appearing features is highlighted with a dashed circle.

Detailed information on the dark appearing features detected in STEM HAADF mode was obtained by EELS. The Ar $L_{2,3}$ edge, with an onset of ~246 eV, can be identified in the spectrum shown in Fig. 5(a), acquired from the dark appearing features. The Ar $L_{2,3}$ edge is overlaid, however, by the tail of the Mo $M_{4,5}$ edge. The signal of the Ar $L_{2,3}$ edge is absent in the dashed lined EEL spectra of the Mo_2BC matrix. However, no remarkable differences can be observed by comparing the acquired EELS edges of the four coatings.

A similar trend is detected in Fig. 5(b) depicting the B K edge. The signals look different according to the probed sample regions (dark appearing feature or Mo_2BC matrix), but are similar within the measurement series (Coating_380 to Coating_630). The B K edge in the Ar containing clusters exhibits two peaks, which are separated by an energy loss of approximately 8 eV. The first peak arises at an energy loss of ~192.5 eV, the second broader one at ~200.5 eV. For Coating_580 and Coating_630 the second peak is slightly shifted to higher energy losses compared to the same peak for the lower T_s coatings. The onset of the B K edges measured in the Mo_2BC matrix (see dashed lined spectra) is located at an energy loss of ~188 eV and shows a less defined electron energy loss near edge structure (ELNES). The C K edges and the Mo

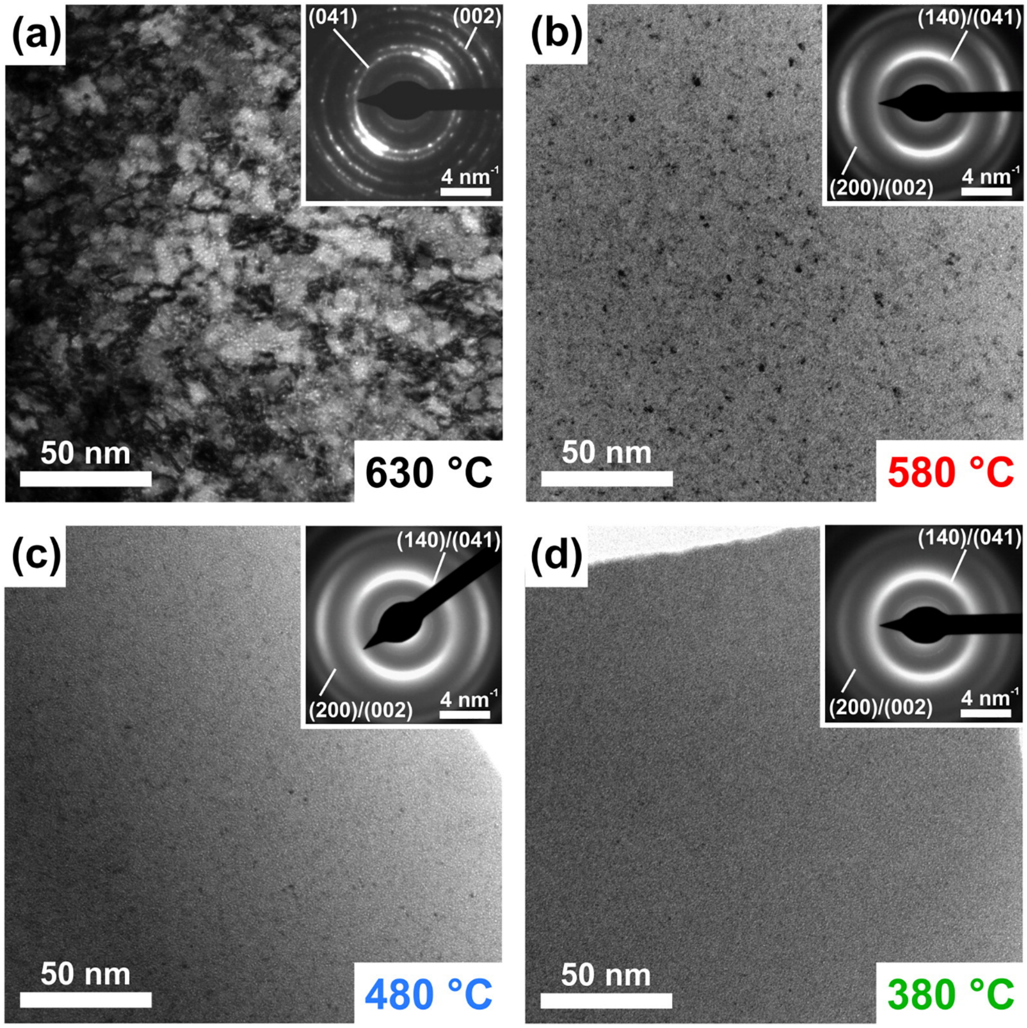

Fig. 3. BF TEM micrographs of Mo_2BC coatings in plan-view deposited at different T_s: (a) 630 °C, (b) 580 °C, (c) 480 °C, and (d) 380 °C. An SAED pattern of each coating from a representative region in plan-view is displayed as inset.

$M_{4,5}$ as well as the Mo $M_{2,3}$ edges were also detected in each coating, but do not reveal significant differences, neither between the Mo_2BC matrix and the dark appearing feature nor as a function of T_s. However, these edges suffer from overlapping of previous edges, which makes interpretation more challenging. The relative sample thicknesses determined with the aid of the corresponding low loss spectra (measurements were performed in dual EELS mode) in the Ar-rich clusters and in the Mo_2BC matrix of all four coatings are between 0.2 and 0.4 times the inelastic mean free path. Estimating an inelastic mean free path of 100 nm for Mo_2BC, the average sample thickness is ~30 nm.

Furthermore, elemental mapping in STEM EELS mode was performed on a dark appearing feature and next to it in the Mo_2BC matrix (see area marked with a rectangle highlighted in white in the left micrograph in Fig. 5(c)). The displayed results in Fig. 5(c) show a representative measurement acquired in the Mo_2BC coating deposited at $T_s = 580$ °C. Ar is the predominantly identified element in the dark appearing feature. In addition, Mo, B, and C are detected, however, the Mo signal is weaker in the region of the dark appearing feature. The STEM HAADF micrograph on the right side of Fig. 5(c) shows the probed scan area after the measurement, indicating beam damage.

Quantitative size analysis of the Ar-rich Mo-B-C clusters was performed by analyzing STEM HAADF micrographs of the four coatings in plan-view. The average Ar-rich Mo-B-C cluster size (in diameter) is 1.5 $\pm$ 0.3 nm for Coating_630, 1.7 $\pm$ 0.3 nm for Coating_580, 1.4 $\pm$ 0.3 nm for Coating_480, and 1.4 $\pm$ 0.2 nm for Coating_380. A distribution curve of the size of 500 analyzed Ar-rich Mo-B-C clusters per coating is shown in Fig. 6(a). The relative Ar-rich cluster amount is displayed in Fig. 6(b). The obtained values represent the amount of Ar-rich Mo-B-C clusters detected in a defined sample area, since a STEM micrograph corresponds to a two-dimensional projection of a three-dimensional object. Taking into account the calculated average sample thickness of the analyzed TEM samples estimated by EELS (~30 nm) and assuming spherical Ar-rich clusters, the volume fraction of the Ar-rich clusters can be estimated and is 0.44 $\pm$ 0.15% for Coating_630, 0.72 $\pm$ 0.09% for Coating_580, 0.62 $\pm$ 0.24% for Coating_480, and 0.73 $\pm$ 0.14% for Coating_380.

In Fig. 7(a), hardness and Young's modulus values of the four coatings, determined by nanoindentation, are summarized. The room temperature hardness values increase as a function of T_s as follows: 21.3 $\pm$ 0.4 GPa (380 °C), 22.8 $\pm$ 0.6 GPa (480 °C), 25.3 $\pm$ 0.7 GPa (580 °C), and 27.9 $\pm$ 1.2 GPa (630 °C). The same trend can be identified for the Young's modulus values, which are corrected for the substrate influence by applying the method of Hay and Crawford [9]. The Young's modulus values taking into account the elastic properties of Si are 259 $\pm$ 10 GPa for Coating_380, 273 $\pm$ 5 GPa for Coating_480, 397 $\pm$ 6 GPa for Coating_580, and 462 $\pm$ 9 GPa for Coating_630. The Young's modulus of Coating_630 is in the range of a fully crystalline and defect-free Mo_2BC (470 GPa) [1]. The ratio of hardness and Young's modulus as a function of T_s, displayed in Fig. 7(b), decreases with increasing T_s.

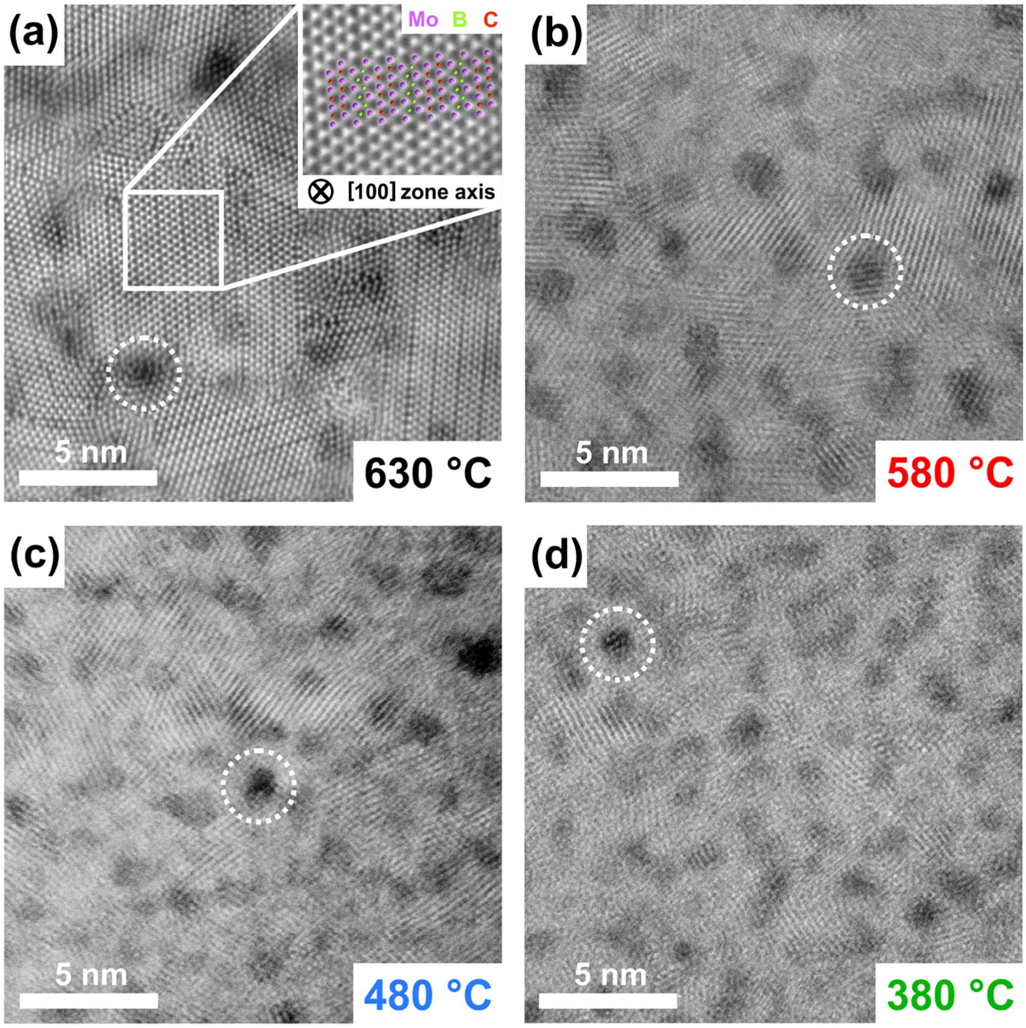

Fig. 4. STEM HAADF micrographs of Mo_2BC coatings in plan-view deposited at different T_s: (a) 630 °C, the inset shows the atom columns of Mo_2BC in [100] viewing direction in higher magnification; (b) 580 °C, (c) 480 °C, and (d) 380 °C. The dashed circles highlight Ar-rich clusters detected in all four analyzed samples.

4. Discussion

The value of T_s has a significant influence on the nanostructure of the deposited coatings as revealed by XRD and TEM investigations. Similar to the results in this study, Bolvardi et al. [2] detected an improvement of crystal quality of Mo_2BC films deposited by HPPMS and DCMS with increasing substrate temperature (in a temperature range from 300 °C to 700 °C) using XRD. It is reasonable to assume that the mobility of condensed plasma species increases with rising T_s, resulting in the formation of coatings with a higher degree of crystallinity and a lower amount of amorphous matrix. This effect is enhanced by ion bombardment induced surface diffusion due to the applied bias voltage of −100 V. A significant difference in the nanostructure of Coating_630 compared to the coatings synthesized at lower T_s can be detected. It may be speculated that an increase in T_s from 580 °C to 630 °C overcomes a kinetic barrier, enabling the growth of a dense array of columnar, crystalline grains in a preferred [100] growth direction. Moreover, small deviations in the stoichiometry of the coatings may influence the nanostructure decisively. Focusing on the elemental composition of the four Mo_2BC coatings, as determined by ERDA, the coating compositions approach the nominal stoichiometry of Mo_2BC with increasing T_s. In the case of Coating_380, an excess of Mo and B, but a lack of C can be detected. In contrast, Coating_630 exhibits a chemical formula of $Mo_{2.0}B_{1.0}C_{0.9}$, which is very close to the nominal stoichiometry of Mo_2BC. Buršík et al. [3] analyzed magnetron sputtered Mo-B-C coatings on a hard metal substrate using a compound Mo_2BC target as well as a combination of three targets, including Mo, C, and B_4C. The coatings deposited with the compound target showed an off-stoichiometric composition and a fully amorphous nanostructure. The coatings deposited with the combination of three targets exhibited a partially crystalline structure with a nanocomposite nature and approached the nominal stoichiometry of Mo_2BC. Thus, it may be speculated that a ratio of Mo:B:C, which is close to the nominal stoichiometry of Mo_2BC, is required in order to form a long-range ordered crystal structure of Mo_2BC, as can be detected in Coating_630. Even a slight deviation in the chemical composition of a Mo_2BC coating deposited at $T_s = 630$ °C is detectable in the form of stacking faults, revealed in a previous study [7].

The applied deposition parameters have an influence on the amount of incorporated Ar working gas in the Mo_2BC coating structure. A negative bias voltage of −100 V and a substrate temperature T_s of at least 380 °C enables the incorporation of Ar ions from the working gas into the coating structure. Moreover, sufficient energy is supplied to enable diffusion of Ar in the subsurface region to locally form Ar-rich Mo-B-C clusters. These clusters have a similar size in all four analyzed coatings within the limits of error. However, the amount of incorporated Ar decreases with increasing T_s, as revealed by ERDA (see Table 2). Similarly, the Ar-rich cluster volume fraction deduced from STEM and EELS analysis (see Fig. 6(b)) decreases with increasing T_s. Thus, an increase of T_s from 380 °C to 630 °C may facilitate desorption of Ar during the growth process, resulting in a lower amount of Ar in the coating.

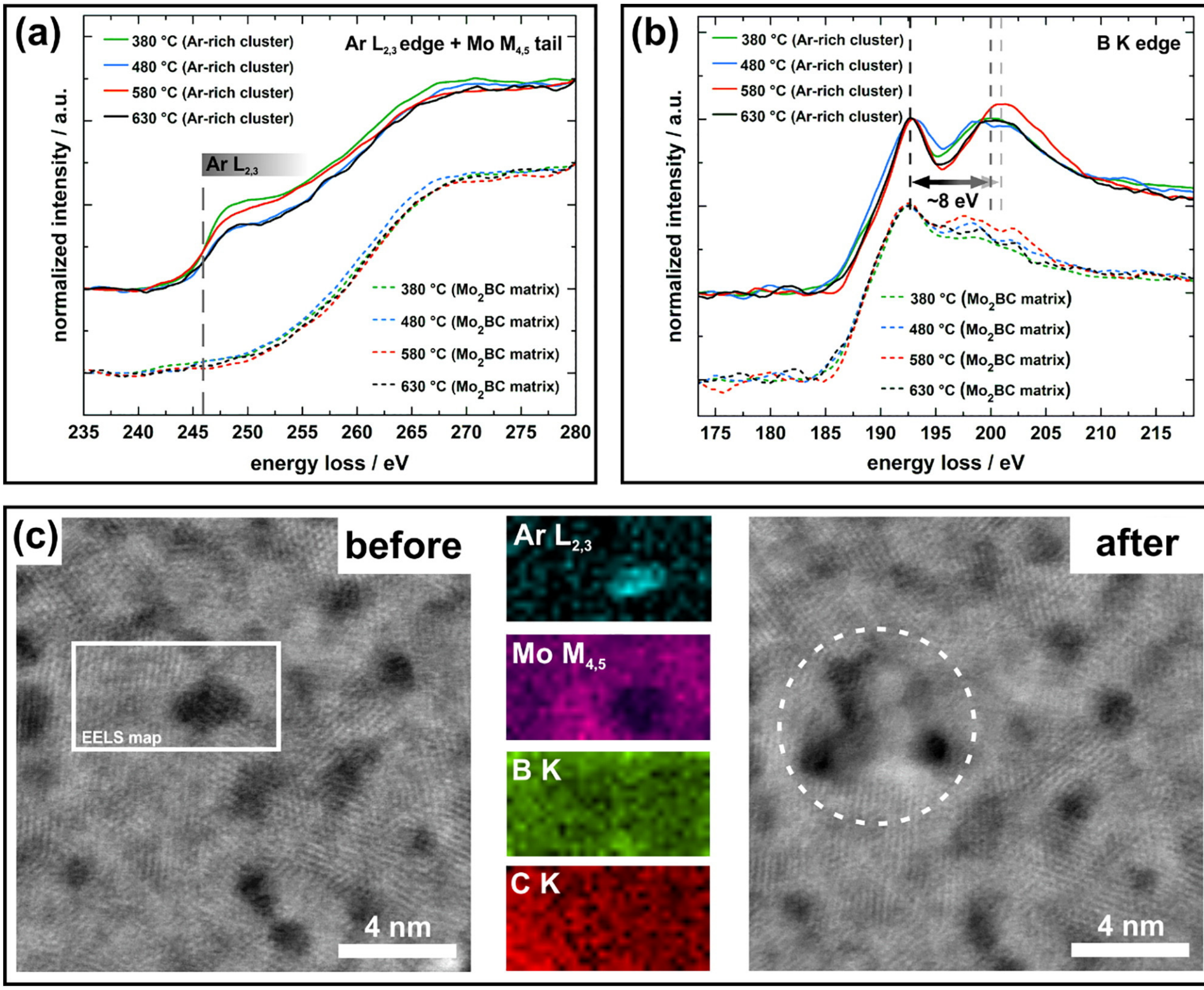

Fig. 5. (a) EEL spectra showing the Ar $L_{2,3}$ and Mo $M_{4,5}$ tail, recorded in an Ar-rich Mo-B-C cluster (continuous line) and in the Mo_2BC matrix (dashed line). (b) EEL spectra, recorded in an Ar-rich Mo-B-C cluster (continuous line) and in the Mo_2BC matrix (dashed line), showing the B K edge. (c) EELS map of a representative Ar-rich Mo-B-C cluster, acquired in the Mo_2BC coating deposited at $T_s = 580$ °C. The EELS map was taken within the white rectangle (see left STEM HAADF micrograph). The scanned region after acquisition of the EELS map is shown in the right STEM HAADF micrograph (see dashed circle).

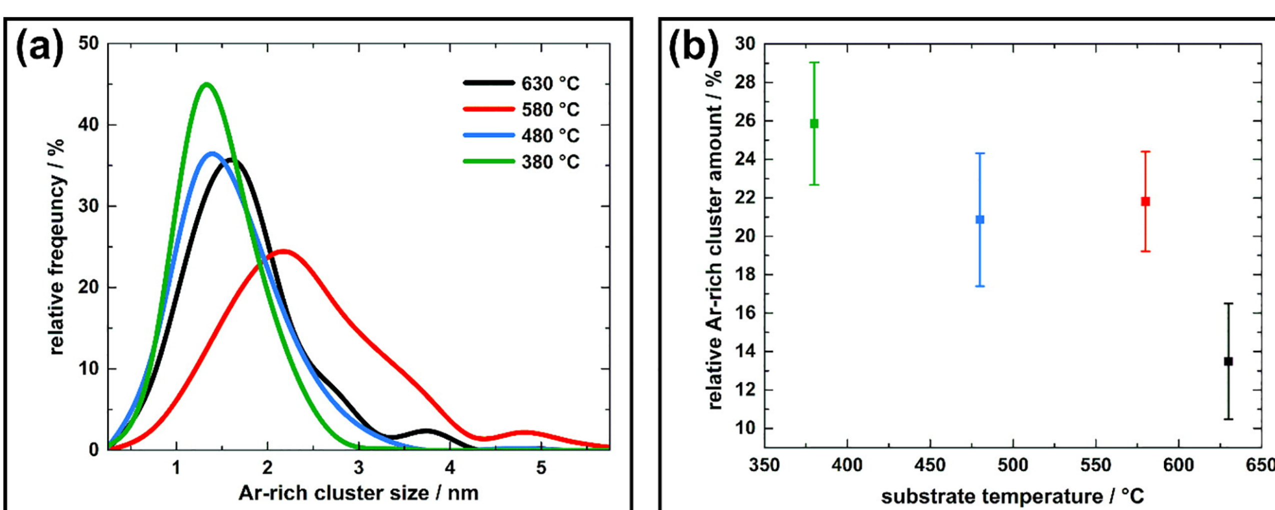

Fig. 6. (a) Ar-rich cluster size (in diameter) distribution obtained by STEM HAADF analysis. (b) Relative amount of Ar-rich Mo-B-C clusters in the analyzed Mo_2BC coatings obtained by STEM HAADF analysis. Color code: Coating_630 (black), Coating_580 (red), Coating_480 (blue), and Coating_380 (green).

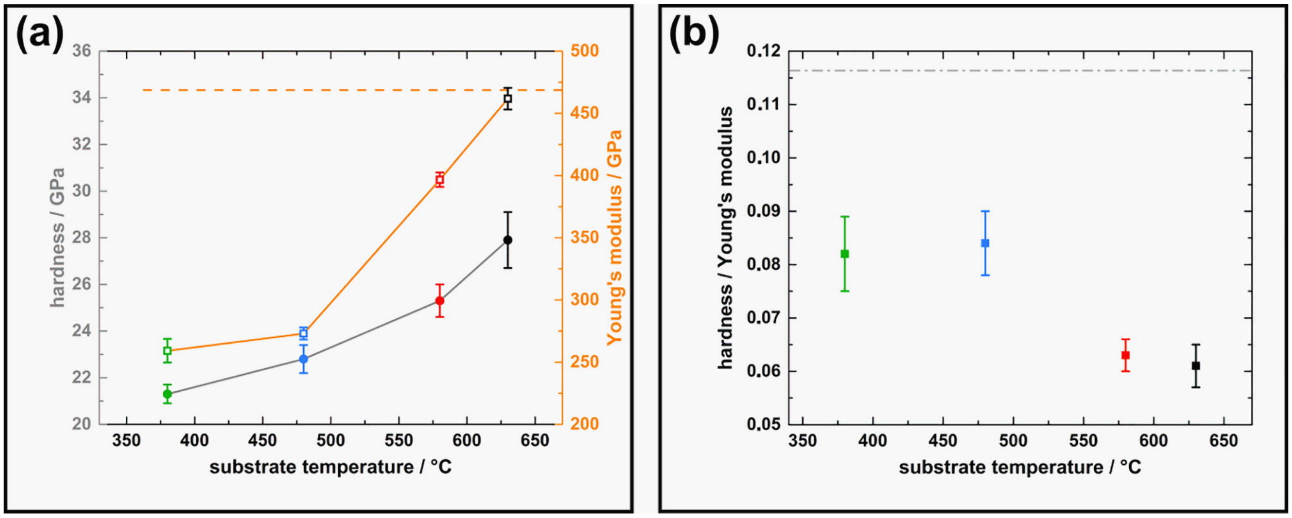

Fig. 7. (a) Hardness (filled symbols) and Young's modulus after substrate influence correction (open symbols) of Mo_2BC as a function of T_s, obtained by nanoindentation. The calculated Young's modulus for fully crystalline and defect-free Mo_2BC is marked with a orange-colored dashed line [1]. (b) Hardness over Young's modulus as a function of T_s. The maximum theoretical hardness for a given Young's modulus is highlighted with a grey-colored dashed line [20].

Moreover, these results indicate that Ar incorporation due to the TEM sample preparation process can be neglected as a possibility. If the Ar had originated from final Ar ion thinning, the amount of dark appearing features, corresponding to Ar-rich Mo-B-C clusters, would have been similar in all four coatings.

The local electronic structure is different in the Ar-rich Mo-B-C clusters compared to the Mo_2BC matrix, as depicted by the EEL spectra of the B K edge and the Ar $L_{2,3}$ edge in Fig. 5. In particular, the chemical environment of B is different, as shown for a Mo_2BC coating deposited on a Si (100) substrate at $T_s = 630$ °C [7]. Focusing on the spectra of the B K edge acquired in the Ar-rich clusters, the ELNES of Coating_380 (green), Coating_480 (blue) and Coating_580 (red), consisting of two peaks separated by an energy loss of approximately 8 eV, are similar to that of Coating_630 (black). These two peaks were identified as π^* and σ^* peaks in a previous study, suggesting a predominant sp^2 hybridization of the B atoms [7]. In contrast, rather featureless ELNES tails can be detected in the B K EEL spectra measured in the Mo_2BC matrix, suggesting a continuous band of unoccupied states [7]. The HAADF micrograph in Fig. 5(c) shows an Ar-rich Mo-B-C cluster after being probed with the electron beam, indicating beam damage. If one considers beam damage as a measure for bond strength, the local bond strength in the Ar-rich Mo-B-C clusters is weaker than in the Mo_2BC matrix. However, significant differences in the electronic structure induced by T_s cannot be detected by EELS, neither in the Ar-rich Mo-B-C clusters, nor in the Mo_2BC matrix. Thus, it may be speculated that the evolution of the nanostructure as a function of T_s, which at least involves a slight change in the electronic structure, is below the resolution limit of our EELS measurements.

The Young's modulus of Mo_2BC increases with rising T_s. Coating_630 has a Young's modulus of 462 ± 9 GPa, which is in good agreement with the *ab initio* calculated value of 470 GPa for a defect free and fully crystalline Mo_2BC structure [1,21]. In addition, the obtained Young's modulus value for $T_s = 630$ °C is in the range of the Young's modulus measured by Emmerlich et al. for a Mo_2BC coating deposited on a α-Al_2O_3 (0001) substrate at $T_s = 900$ °C (460 ± 21 GPa) [1]. However, even in Coating_630, the grain boundary regions exhibit an atomic arrangement which is less ordered, but the volume fraction of crystalline matter to less ordered grain boundary regions is the highest in this coating. Thus, the average bond strength is higher in Coating_630 than for the lower T_s coatings, where short-range ordered matter dominates. The short-range ordered matter is characterized by a distribution in bond lengths that generally results in lower stiffness compared to the corresponding crystalline phase [22]. Moreover, the incorporation of Ar may reduce the average bond strength as Ar is not expected to contribute towards the formation of ionic or covalent bonds, resulting in a further decrease in stiffness and therefore in a lower Young's modulus. For the four analyzed Mo_2BC coatings, the amount of Ar in Coating_380 is almost twice that in Coating_630.

Coating_630, with a hardness of 28 GPa, exhibits the highest hardness value of the coatings analyzed in this study. This is in accordance with hardness values of similarly synthesized Mo_2BC coatings reported in literature (29 GPa [1], 31.6 GPa [3,4]). The trend of increasing hardness with rising T_s was previously observed for TiN by Combadiere and Machet [23], Hibbs et al. [24], and Münz and Hessberger [25] as well as for TiC by Jacobsen et al. [26] A similar trend was also found by Buršík et al. [3] and Zábranský et al. [4] who analyzed the effect of different deposition parameters on Mo_2BC coatings. Taking into account the results of TEM, including SAED and STEM HAADF, we conclude that a rise in T_s increases the degree of crystallinity in the coating, which results in higher hardness values. An increasing degree of crystallinity involves an increase in grain size and in the ratio of crystalline regions to amorphous matter as well as an evolving columnar grain structure with a preferred grain orientation.

Finally, a decreasing ratio of hardness to Young's modulus with increasing T_s can be detected, as displayed in Fig. 7(b). Kauffmann et al. [20] derived a linear relation to calculate the maximum theoretical hardness of a hard coating, which is around 12% of the measured Young's modulus. By applying the relation to Coating_630, which exhibits a Young's modulus of 462 ± 9 GPa, a theoretical hardness of around 50 GPa is expected. Since the experimentally determined hardness is >20 GPa lower than this value, and the corresponding hardness to Young's modulus ratio is ~0.06, irreversible deformation must occur, either due to cracking or plasticity. As no indication of cracking is detected by nanoindentation, it is reasonable to assume that the reduced hardness over Young's modulus value originates from plasticity. According to Emmerlich et al. [1] easy glide directions exist in crystalline Mo_2BC. The (040) and (080) planes, in particular, can enable plasticity, as dislocation mobility is high along these planes, while stiff, amorphous phases may plastically deform by shear bending [27,28]. The hardness over Young's modulus value increases with decreasing T_s, as the amount of crystalline phase is reduced and thus, plasticity is increasingly suppressed.

5. Conclusions

In this study, we demonstrated how the substrate temperature T_s controls the nanostructure and thus the mechanical properties of

Mo_2BC hard coatings. The coatings were deposited on Si (100) substrates by bipolar pulsed DCMS at different substrate temperatures, ranging from 380 °C to 630 °C. With respect to mechanical properties we showed that a substrate temperature of 380 °C is sufficient to achieve a reasonable hardness (21 ± 1 GPa) and Young's modulus (259 ± 10 GPa). An increase of T_s up to 630 °C leads to an increase in hardness up to 28 ± 1 GPa and in Young's modulus up to 462 ± 9 GPa. These results can be explained by our XRD and TEM findings. The ratio of crystalline regions to short-range ordered, amorphous matter increases with increasing T_s. Moreover, columnar grain growth evolves with increasing T_s. We were able to show that Ar from the working gas is incorporated in each coating as Ar-rich Mo-B-C clusters. The volume fraction of these clusters was determined by TEM and shows a decrease with rising T_s. Despite these defects, high hardness and Young's modulus values were obtained. Elemental composition analysis obtained by ERDA revealed that coating compositions approach the nominal stoichiometry of Mo_2BC with increasing T_s, facilitating the crystalline phase formation.

Acknowledgements

The authors would like to thank Benjamin Breitbach for performing the XRD measurements and Christoph Kirchlechner for valuable discussions. Jochen M. Schneider acknowledges financial support by the German Science Foundation (DFG) *via* the project SCHN 735/35-1 and funding from the MPG fellow program. Moreover, financial support from the DFG *via* the project DE 796/10-1 is gratefully acknowledged by Rafael Soler and Gerhard Dehm.

References

[1] J. Emmerlich, D. Music, M. Braun, P. Fayek, F. Munnik, J.M. Schneider, A proposal for an unusually stiff and moderately ductile hard coating material: Mo_2BC, J. Phys. D. Appl. Phys. 42 (18) (2009) 1–6.
[2] H. Bolvardi, J. Emmerlich, S. Mraz, M. Arndt, H. Rudigier, J.M. Schneider, Low temperature synthesis of Mo_2BC thin films, Thin Solid Films 542 (2013) 5–7.
[3] J. Buršík, V. Buršíková, P. Souček, L. Zábranský, P. Vašina, Nanostructured Mo-B-C coatings, Rom. Rep. Phys. 68 (3) (2016) 1069–1075.
[4] L. Zábranský, V. Buršíková, P. Souček, P. Vašina, J. Buršík, On the study of the mechanical properties of Mo-B-C coatings, Eur. Phys. J. Appl. Phys. 75 (2) (2016) 24716/1–24716/7.
[5] V. Buršíková, J. Sobota, J. Grossman, T. Fořt, L. Dupák, L. Zábranský, P. Souček, P. Vašina, J. Buršík, Study of Fracture Resistance of Nanolaminate Coatings Using Indentation and Impact Tests, 258, 2017 318–321.
[6] L. Zábranský, V. Buršíková, P. Souček, P. Vašina, J. Dugáček, P. Stahel, J. Buršík, M. Svoboda, V. Peřina, Thermal stability of hard nanocomposite Mo-B-C coatings, Vacuum 138 (2017) 199–204.
[7] S. Gleich, H. Fager, H. Bolvardi, J.-O. Achenbach, R. Soler, K.G. Pradeep, J.M. Schneider, G. Dehm, C. Scheu, Nano and defect structure analysis in a Mo_2BC hard coating investigated by transmission electron microscopy and atom probe tomography, J. Appl. Phys. 122 (7) (2017) 075305/1–075305/9.
[8] W.C. Oliver, G.M. Pharr, An improved technique for determining hardness and elastic-modulus using load and displacement sensing indentation experiments, J. Mater. Res. 7 (6) (1992) 1564–1583.
[9] J. Hay, B. Crawford, Measuring substrate-independent modulus of thin films, J. Mater. Res. 26 (6) (2011) 727–738.
[10] J.J. Wortman, R.A. Evans, Young's modulus, shear modulus, and Poisson's ratio in silicon and germanium, J. Appl. Phys. 36 (1) (1965) 153–156.
[11] J. Scott, P.J. Thomas, M. Mackenzie, S. McFadzean, J. Wilbrink, A.J. Craven, W.A. Nicholson, Near-simultaneous dual energy range EELS Spectrum imaging, Ultramicroscopy 108 (12) (2008) 1586–1594.
[12] R.F. Egerton, Electron energy-loss spectroscopy in the TEM, Rep. Prog. Phys. 72 (1) (2009) 016502/1–016502/25.
[13] A. Savitzky, M.J.E. Golay, Smoothing and differentiation of data by simplified least squares procedures, Anal. Chem. 36 (8) (1964) 1627–1639.
[14] A. Strecker, U. Salzberger, J. Mayer, Specimen preparation for transmission electron microscopy (TEM): reliable method for cross sections and brittle materials, Prakt. Metallogr. 30 (10) (1993) 482–495.
[15] P. Ström, P. Petersson, M. Rubel, G. Possnert, A combined segmented anode gas ionization chamber and time-of-flight detector for heavy ion elastic recoil detection analysis, Rev. Sci. Instrum. 87 (10) (2016) 103303/1–103303/6.
[16] M.S. Janson, CONTES Conversion of Time-Energy-Spectra - A Program for ERDA Data Analysis, Internal Report, Uppsala University, 2004.
[17] M. to Baben, M. Hans, D. Primetzhofer, S. Evertz, H. Ruess, J.M. Schneider, Unprecedented thermal stability of inherently metastable titanium aluminum nitride by point defect engineering, Mater. Res. Lett. 5 (3) (2017) 158–169.
[18] M.A. Arvizu, R.T. Wen, D. Primetzhofer, J.E. Klemberg-Sapieha, L. Martinu, G.A. Niklasson, C.G. Granqvist, Galvanostatic ion detrapping rejuvenates oxide thin films, ACS Appl. Mater. Interfaces 7 (48) (2015) 26387–26390.
[19] E. Rudy, F. Benesovsky, L. Toth, Untersuchung der Dreistoffsysteme der Va- und VIa-Metalle mit Bor und Kohlenstoff, Z. Met. 54 (6) (1963) 345–353.
[20] F. Kauffmann, G. Dehm, V. Schier, A. Schattke, T. Beck, S. Lang, E. Arzt, Microstructural size effects on the hardness of nanocrystalline TiN/amorphous-SiNx coatings prepared by magnetron sputtering, Thin Solid Films 473 (1) (2005) 114–122.
[21] H. Bolvardi, J. Emmerlich, M. to Baben, D. Music, J. von Appen, R. Dronskowski, J.M. Schneider, Systematic study on the electronic structure and mechanical properties of X_2BC (X = Mo, Ti, V, Zr, Nb, Hf, Ta and W), J. Phys. Condens. Matter 25 (4) (2013) 045501/1–045501/6.
[22] D. Music, F. Hensling, T. Pazur, J. Bednarcik, M. Hans, V. Schnabel, C. Hostert, J.M. Schneider, Bonding and elastic properties of amorphous AlYB14, Solid State Commun. 169 (2013) 6–9.
[23] L. Combadiere, J. Machet, Reactive magnetron sputtering deposition of TiN films. II. Influence of substrate temperature on the mechanical properties of the films, Surf. Coat. Technol. 88 (1–3) (1997) 28–37.
[24] M.K. Hibbs, B.O. Johansson, J.E. Sundgren, U. Helmersson, Effects of substrate-temperature and substrate material on the structure of reactively sputtered TiN films, Thin Solid Films 122 (2) (1984) 115–129.
[25] W.D. Munz, G. Hessberger, Beschichtung von Formteilen mit TiN durch Hochleistungskathodenzerstäubung, Vakuum-Technik 30 (3) (1981) 78–86.
[26] B.E. Jacobson, R.F. Bunshah, R. Nimmagadda, Transmission electron microscopy studies of TiC and VC-TiC deposits prepared by activated reactive evaporation, Thin Solid Films 54 (1) (1978) 107–118.
[27] M.M. Trexler, N.N. Thadhani, Mechanical properties of bulk metallic glasses, Prog. Mater. Sci. 55 (8) (2010) 759–839.
[28] V. Schnabel, B.N. Jaya, M. Kohler, D. Music, C. Kirchlechner, G. Dehm, D. Raabe, J.M. Schneider, Electronic hybridisation implications for the damage-tolerance of thin film metallic glasses, Sci. Rep. 6 (2016) 36556/1–36556/12.